*Article*

# Experimental Investigation on the Characteristic Mobilization and Remaining Oil Distribution under CO$_2$ Huff-n-Puff of Chang 7 Continental Shale Oil

Jianhong Zhu [1,2], Junbin Chen [1,2,*], Xiaoming Wang [1,2], Lingyi Fan [1,2] and Xiangrong Nie [1,2,*]

1    College of Petroleum Engineering, Xi'an Shiyou University, Xi'an 710065, China;
     19111010002@stumail.xsyu.edu.cn (J.Z.); 18109071005@stu.xust.edu.cn (X.W.);
     19211010006@stumail.xsyu.edu.cn (L.F.)
2    Shaanxi Key Laboratory of Well Stability and Fluid & Rock Mechanics in Oil and Gas Reservoirs,
     Xi'an Shiyou University, Xi'an 710065, China
*    Correspondence: chenjb@xsyu.edu.cn (J.C.); xrnie@xsyu.edu.cn (X.N.); Tel.: +86-029-8973-2268 (J.C. & X.N.)

**Abstract:** The Chang 7 continental shale oil reservoir is tight. The recovery factor is extremely low, the remaining oil is very high, and injecting water to improve oil recovery effectiveness is too hard. Therefore, in this paper, physical simulation experiments of CO$_2$ huff-n-puff shale oil and NMR tests were conducted to study the cycle numbers and permeability on the recovery degree, as well as the characteristics of shale oil mobilization and the remaining oil micro distribution. The results showed that the cumulative oil recovery factors (ORFs) gradually increased in the natural logarithmic form, the single cycle ORFs decreased rapidly in exponential form with the huff-n-puff cycle number, and the biggest economic cycle numbers were between approximately 3 and 5. Furthermore, the higher the permeability, the higher the ORF, but the difference of ORF decreased between the two experimental samples with the cycles. In addition, the gap of production and recovery degree was large between the different scale pores, the ORF of macropores was 6–8 times that of micropores, and the final remaining oil was mainly distributed in the micropores, accounting for 82.29% of the total amount; meanwhile, the macropores comprised less than 0.5%. In the process of huff-n-puff, CO$_2$ flowed into macropores, mesopores, and smallpores under the pressure differential effect, but a small amount of CO$_2$ slowly diffused into micropores, resulting in the ORF of the former with more free oil being higher and the ORF of micropores with more adsorbed oil being lower. Therefore, promoting a better contact and reaction between CO$_2$ and shale oil of micropores is one of the key ways to effectively develop the Chang 7 continental shale oil and enhance oil recovery.

**Keywords:** CO$_2$ huff-n-puff; oil recovery factor; remaining oil distribution; NMR; pore scale

## 1. Introduction

In recent years, global oil and gas consumption has been increasing. However, the remaining reserves of conventional resources have decreased with exploration and development, resulting in a scarcity of energy. As a result, unconventional resources (such as tight/shale oil and gas) will play an extremely significant role in the petroleum industry. According to the assessment results of the US Energy Information Administration (EIA, 2019), the technical recoverable resources of shale oil in the world are about $473 \times 10^8$ t, and the US shale oil production reached $3.20 \times 10^8$ t, which accounted for 64.7% of the total oil production in 2018 [1,2]. The exploration results showed that China has abundant shale oil geological reserves of $1420 \times 10^8$ t, and the amount of medium and high maturity continental shale oil with good development prospects is about $200 \times 10^8$ t [3–5]. However, there are issues regarding depletion developments, such as the low production of an individual well, rapid decline, and ultra-low recovery (generally below 10%) [6,7]. Therefore, there is imperative to investigate enhanced oil recovery (EOR) technology for the further development of shale oil reservoirs.

Compared with water flooding, injecting gas can improve shale oil recovery because the viscosity of water is higher than gas, and shale oil reservoirs have ultra-low porosity and permeability characteristics, as well as containing a higher clay content that is prone to absorb water and expand. These factors result in a high injection pressure and a low water injection. Sheng et al. [8,9] simulated different water and gas injection schemes combined with the field production data of shale reservoirs. The results showed that whatever the waterflooding, the water injection volume and recovery factor were very low, but the effect of gas injection was better. Additionally, the recovery factor of gas huff-n-puff was higher than continuous injection, and the difference between them could be as high as 32.46%, which indicated that gas huff-n-puff was a more effective development technology suitable for shale reservoirs. However, for selecting an appropriate gas, Khalid E., Gamadi, and Jia B. et al. [10–14] made comparative analyses of the development effects for multiple factors through physical simulation laboratory experiments, such as injection gas (such as $CO_2$, $N_2$, $C_1$, and $C_2$), displacement methods (such as gas flooding, huff-n-puff, and WAG), shut-in time, cycle numbers, injection pressure, production time. The results showed that the ORF of $CO_2$ injection was better than others and improved about 10–50%. Furthermore, $CO_2$ has the characteristics of a wide distribution, safety, and reliability. Additionally, it has great environmental and social significance to inject $CO_2$ into a shale oil reservoir, which can alleviate the greenhouse effect to a certain extent.

The mechanism of $CO_2$ EOR in tight/shale reservoirs has been investigated by numerous studies. Weijermars R. and Nandlal K. et al. [15] suggested that one of the principal mechanisms of EOR by gas injection is pressurizing the dead fluid zones between fractures, and the minimum miscibility pressure (MMP) between $CO_2$ and oil may be reached with reservoirs deeper than 3000 ft. Additionally, huff-n-puff $CO_2$ EOR is best applied in shale wells when the transition of the flow regime presented on diagnostic plots occurs. Ho Tuan A. and Wang Y. [16] used the molecular dynamics simulation method to find that supercritical $CO_2$ can affect shale oil in both inorganic and organic nanopores, but water only works in inorganic nanopores. H. Yu [17] found that $CO_2$ huff-n-puff could more effectively improve oil recovery for shale with an ultra-low permeability through the numerical simulation method. Gamadi and Li L. et al. [18,19] used a component simulator to analyze the effects of reservoir heterogeneity, soaking time, injection pressure, and huff-n-puff cycles on EOR. Wan et al. [20,21] indicated that molecular diffusion was the significant mechanism of EOR via a $CO_2$ injection numerical simulation with single porosity model and dual permeability model in Eagle Ford shale oil. Gamadi et al. [22] carried out $CO_2$ huff-n-puff experiments and decided that diffusion and dragging were the important mechanisms of EOR based on Mancos and Eagle Ford shale core. For the reservoir characteristics of tight/shale oil in China, Zhang Y., Wei B., and X. Wang [23–25] carried out experiments to show that $CO_2$ huff-n-puff could effectively improve production degree.

Though numerous studies have shown that $CO_2$ huff-n-puff is an efficient EOR technology for shale reservoirs, few studies have investigated the production and remaining oil distribution characteristics in natural bedding, micro-fractures, and matrix micro-nano pores. Additionally, the $T_2$ spectrum curve of the relationship between transverse relaxation time and nuclear magnetic signal intensity tested by NMR can quantitatively describe the crude oil content in pores with different sizes. Therefore, NMR has become an effective method to describe the fluid flow in the pores of unconventional reservoirs after $CO_2$ huff-n-puff. In this paper, SEM images were used to analyze the pore structure types and features of Chang 7 continental shale cores. Next, we studied the influence of recovery degree with different cycles and permeabilities through $CO_2$ huff-n-puff lab experiments on continental shale oil and analyzed the pore volume proportions of different scales and the microscopic characteristics of shale oil production and remaining oil distribution combined with the NMR $T_2$ spectrum curves. These can provide theoretical guidance for $CO_2$ huff-n-puff to enhance shale oil recovery.

## 2. Fundamental Theory

### 2.1. Pore Radius Conversion Theory Based on NMR

NMR is a physical process of absorbing a certain radio frequency (RF) that is radiation-resonated, and the resonance is generated when an external magnetic field acts on a nucleus of non-zero magnetic distance to result in the nucleus being self-rotated to cause Zeeman splitting. The $T_2$ spectrum of transverse relaxation time could be obtained by detecting NMR signals in the pores containing oil and water. Then, the fluid distribution in different pore sizes is obtained by a mathematical inversion calculation. In a uniform magnetic field, the formula for $T_2$ can be expressed as the following equation:

$$\frac{1}{T_2} = \frac{1}{T_{2D}} + \frac{1}{T_{2B}} + \frac{1}{T_{2S}} = \frac{D(\gamma G T_E)^2}{12} + \frac{1}{T_{2B}} + \rho \frac{S}{V} \tag{1}$$

where $T_2$ is the total pore fluid transverse relaxation time (ms), $T_{2D}$ is the diffusion relaxation time (ms), $T_{2B}$ is the volume relaxation time that is determined by the self-properties of the fluid (ms), $T_{2S}$ is the surface relaxation time that is related to the pore structure (ms), $\rho$ is the transverse surface relaxivity ($\mu$m/ms), $S$ is the pore surface area ($\mu$m$^2$), $V$ is the pore volume ($\mu$m$^3$), $D$ is the diffusion coefficient (cm$^2$/s), $\gamma$ is the nuclear gyromagnetic ratio, $G$ is the magnetic field gradient (Guss/cm), and $T_E$ is the echo spacing of measurement sequence (ms).

In lab NMR tests, the magnetic field of sets can be nearly uniform, and the magnetic field and echo spacing of measurement sequence can be too small. In this case, the diffusion relaxation $1/T_{2D}$ can be neglected. Moreover, the volume relaxation time $T_{2B}$ depends on the self-properties of fluids. For specific liquids with a low viscosity such as water and light oil, the $T_{2B}$ is very long and a constant under a specific condition. Additionally, the surface relaxation time $T_{2S}$ is proportional to the pore radius, and the pore radius of shale is mainly at the nano and micro scales, resulting in the surface relaxation time $T_{2S}$ being extremely low in shale core. Generally, the volume relaxation time $T_{2B}$ is much larger than the surface relaxation time $T_{2S}$ in shale rock, which means that the $1/T_{2B}$ can also be neglected [26]. Therefore, Equation (1) can be simplified as follows [27]:

$$\frac{1}{T_2} = \rho_2 \frac{S}{V} = \rho_2 \frac{F_S}{r} \tag{2}$$

where $F_s$ is the dimensionless pore shape factor and $r$ is the pore radius ($\mu$m). Equation (2) shows that the $T_2$ value is directly proportional to the pore radius $r$. A previous study [28] found that the relationship between $T_2$ value and pore radius $r$ is a power function according to a large number of experimental data statistics, as seen in the following equation:

$$r = CT_2^n \tag{3}$$

where $C$ and $n$ are the coefficients that can be obtained by conversion from high pressure mercury injection data.

### 2.2. Relationship between $T_2$ Spectrum and the Remaining Oil Content

An NMR $T_2$ spectrum is a relationship curve between transverse relaxation time $T_2$ and NMR signal amplitude. The envelope area of the curve is the total NMR signal amplitude within a certain transverse relaxation time range, which reflects the quantity of $^1$H in fluid. The integral area of a $T_2$ spectrum curve has the following relationship with the mass of fluid in rock:

$$m_o = \alpha S(T_2) \tag{4}$$

where $m_o$ is the fluid mass (g), $S(T_2)$ is the integral area of the $T_2$ spectrum curve comprising the total NMR signal amplitude, and $\alpha$ is the coefficient determined by experiment. The difference of integral areas under the two $T_2$ spectrum curves is the change of fluid mass in the specimen, as shown in Figure 1. Curves 1 and 2 are oil-bearing $T_2$ spectrum curves

before and after the experiment, respectively. The yellow part is the integral area difference between the two curves. Then, the change of oil mass is:

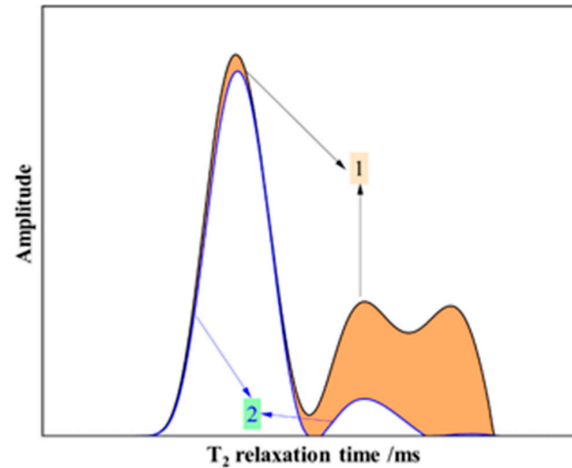$$\Delta m = m_1 - m_2 = \alpha S_1(T_2) - \alpha S_2(T_2) \tag{5}$$



**Figure 1.** NMR $T_2$ spectrum curve of before and after the experiment. **1** denotes the oil-bearing $T_2$ spectrum curves before the experiment, and **2** denotes the oil-bearing $T_2$ spectrum curves after the experiment.

Then the recovery degree $\eta$ can be calculated as follows:

$$\eta = \frac{\Delta m}{m_1} \times 100\% = \frac{S_1(T_2) - S_2(T_2)}{S_1(T_2)} \times 100\% \tag{6}$$

Therefore, after combining the relationship between rock pore radius and transverse relaxation time in Equation (3), one could analyze and calculate the distribution, producing degree, and remaining oil content of shale oil of different pore sizes.

## 3. Experiments

### 3.1. Materials

The experimental core samples in Figure 2 were drilled in the Yanchang 7th Formation of Triassic in Ordos Basin. The continental shale of Chang 7 is a set of source rock series that are mainly composed of shale formed in the heyday of Late Triassic lake basin development. Though the two cores were cut from the same rock specimen, there was still a permeability difference due to the strong reservoir heterogeneity in the shale. Table 1 displays the properties of the core samples.
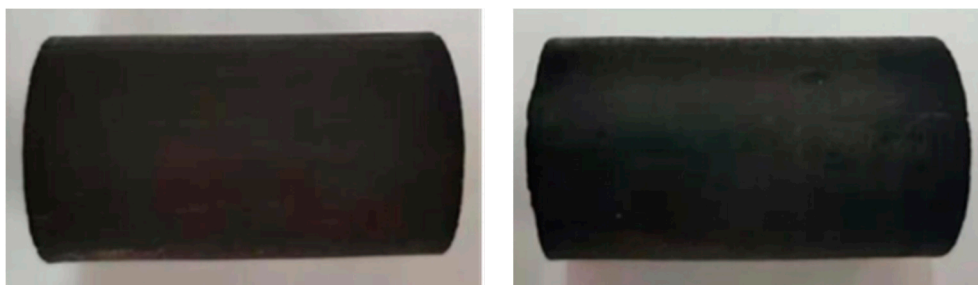


(**a**) Core #Y1         (**b**) Core #Y2

**Figure 2.** Chang 7 formation core samples used in this study.

**Table 1.** Physical properties of the core samples.

| Core No. | Diameter, cm | Length, cm | Porosity, % | Permeability, $10^{-3}$ $\mu m^2$ |
|----------|--------------|------------|-------------|-----------------------------------|
| Core #Y1 | 2.498 | 3.423 | 5.77 | 0.2911 |
| Core #Y2 | 2.500 | 3.573 | 6.06 | 0.0169 |

The oil used in this study was n-dodecane with a density of 0.7487 g/cm$^3$ and a viscosity of 1.508 mPa·s at 25 °C, and the calibration curve between n-dodecane and NMR signal amplitude is shown in Figure 3. The $CO_2$ was from Suzhou Chenggong Co. Ltd., Suzhou, China, with a purity of 99.9%.
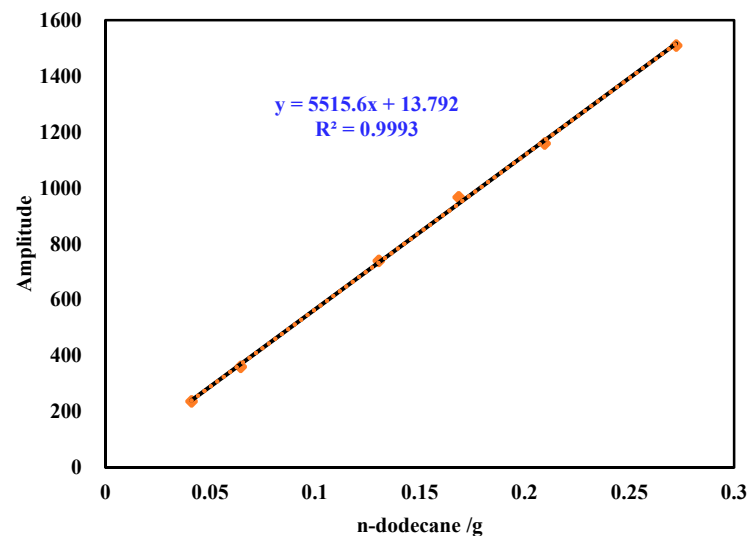


**Figure 3.** The calibration curve of n-dodecane vs. NMR signal amplitude.

### 3.2. Experimental Apparatus

The main experiments carried out in this study were SEM, $CO_2$ huff-n-puff, and NMR tests. The major apparatus for SEM included an argon ion polishing instrument (Ilion+II697C, Gatan Co., Warrendale, PA, USA), an energy spectrometer field emission scanning electron microscope (FESEM, Quanta 450, FEI Co., Hillsboro, OR, USA), and an energy spectrometer (AMETEK, EDAX Co., Philadelphia, PA, USA). As shown in the $CO_2$ huff-n-puff experiment schematic of Figure 4, the huff-n-puff vessel was fitted with $CO_2$ from the cylinder before huff-n-puff. The ISCO pump (260 D, ISCO, Lincoln, NE, USA) provided power to inject $CO_2$ from the plug-type container to the core. The hand pump provided backpressure, and the temperature control setup allowed for the maintenance of the temperature of the whole experimental system at 45 °C during the process. The NMR spectrometer was produced by Suzhou Niumag Analytical Instrument Co., Ltd., Suzhou, China. The magnetic field strength was 0.52 ± 0.05 T, and the resonance frequency of the hydrogen proton was 21.3 MHz. Other devices used in this study included a core linear cutting machine, a core cleaner, an oven, a core measurement system, an analytical electronic balance, a Vernier caliper, and a gas flowmeter.

### 3.3. Experimental Procedures

The experimental procedures were as follows.

(1) Core preparation: we prepared the shale cores by a linear cutting machine with a diameter of 25 mm, and we cleaned the samples for 28 days. Afterwards, they with dried at 120 °C for about 3 days, and the permeability and porosity were tested by helium.

(2) SEM tests: we took the core slice from the standard sample and polished the surface. Then, the polished sample was photographed by FESEM.

(3) Rock sample saturation: we vacuumed the core samples for 72 h. Next, the specimens were saturated with n-dodecane for 48 h at 30 MPa and 45 °C, and then we put them into the container with n-dodecane for one week to completely saturate at 45 °C. Additionally, the samples were weighed before and after the processes.

(4) Initial $T_2$ spectrum: after saturation, we measured the samples with an NMR apparatus to obtain the initial $T_2$ spectrum curves of the saturated oil.

(5) $CO_2$ huff: first, we put the core into the huff-n-puff vessel, and then, as shown in Figure 4, the experimental process was connected. After we filled the huff-n-puff vessel with $CO_2$ from the cylinder, $CO_2$ in the plug-type container was injected into the huff-n-puff vessel by the ISCO pump at 15 MPa.

(6) $CO_2$ puff: all valves were closed during the soaking period for 12 h. We opened valve #3 and controlled the back pressure to gradually drop to 0 MPa.

(7) $CO_2$ huff-n-puff $T_2$ spectrum: we took out the core from the huff-n-puff vessel, and then we weighed the sample by the analytical electronic balance and measured the $T_2$ spectrum using the NMR apparatus.

(8) We repeated steps (5)–(7) at the same injection pressure of 4 rounds for the $CO_2$ huff-n-puff experiments and NMR tests.
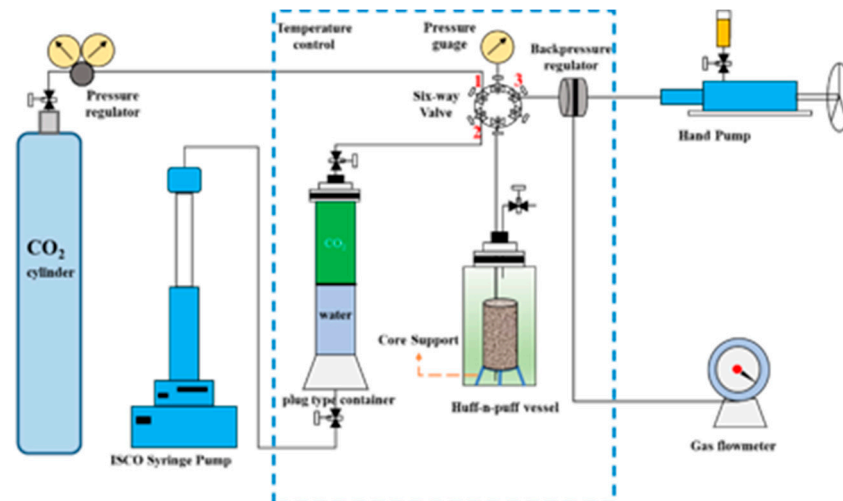


**Figure 4.** Schematic of the apparatus for the $CO_2$ huff-n-puff experiments. The red numbers 1, 2 and 3 denote three different valves in the six-way valve.

## 4. Results and Discussions

### 4.1. Pore Characteristics and Radius Distribution

The SEM images of Chang 7 shale core samples are shown in Figure 5. It could be observed that the rock was tight shale, and microfractures with different lengths and widths, as well as a large number of micropores, were developed. Some larger pores were filled with clastic particles among the minerals, such as pyrite and illite. Hence many micropores were formed. As a whole, massive micro-smallpores and fractures developed, and relatively few large-scale pores were distributed in the rock.
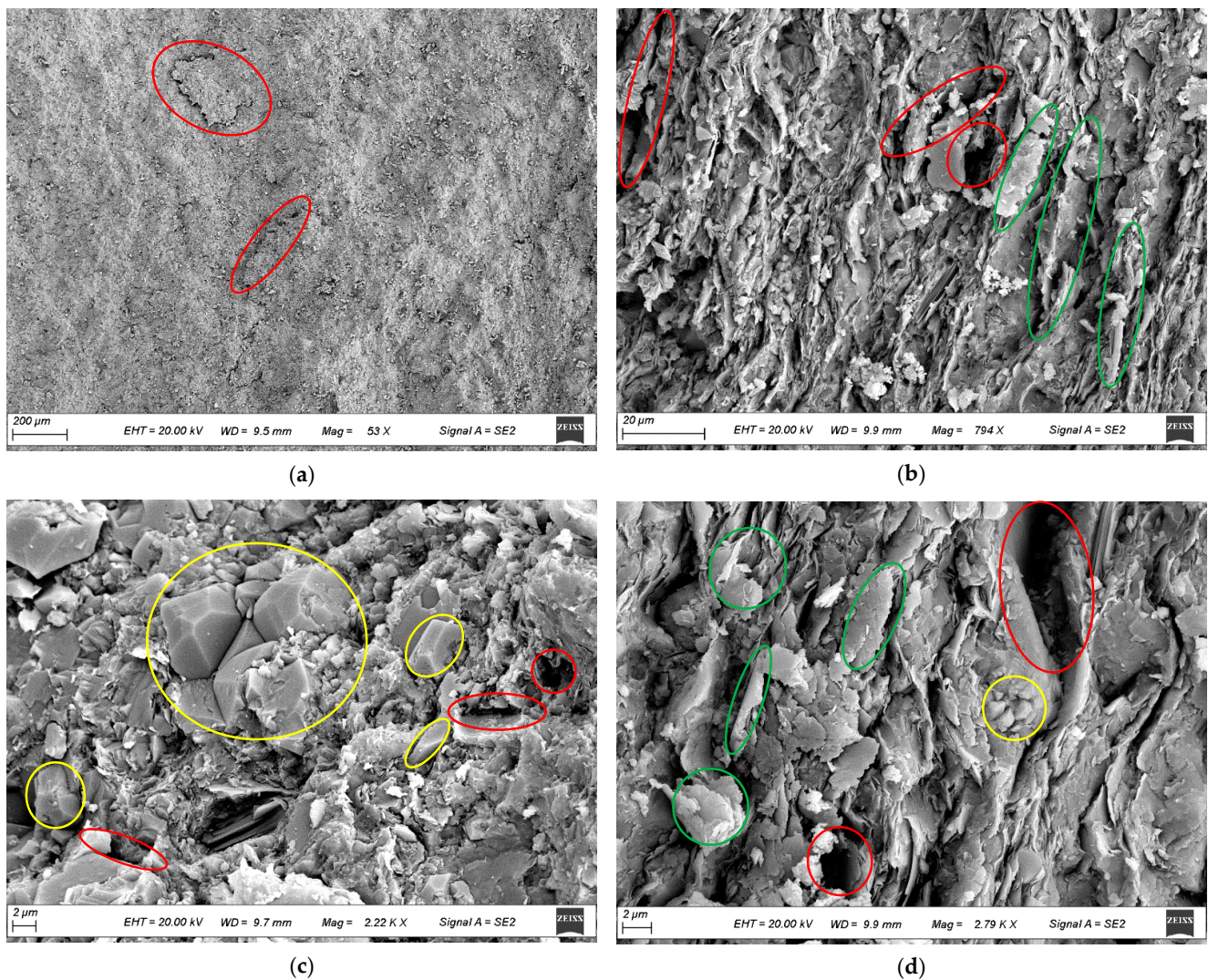
**Figure 5.** SEM images of core samples. (**a**) The full view of SEM image magnified 53 times shows that the rock was tight. (**b**–**d**) The SEM images magnified 794, 2220, and 2790 times show the clay minerals of lamellar illite, crystalline pyrite, and micropores/fractures, respectively. (Note: the red circles are pores and fractures, the yellow circles are crystalline pyrite, and the green circles are illite.).

Figure 6 shows the $T_2$ spectrum curves of initial saturated oil in cores. The curve of core #Y1 has three wave crests, but the transition between the middle and right crest is not apparent in the other one. The crest decreases from left to right, which indicates that the core pore distribution was strongly heterogeneous. The crest on the left means micropores, the middle one means mesopores, the trough between the two means smallpores, and the crest on the right represents macropores or fractures. In the $T_2$ spectrum of core #Y2, there is a little transition between the crests that represents mesopores and macropores. Therefore, after combining this spectrum with Equation (3), the pore radius distribution could be shown in Figure 7. In this study, the shale pores could be divided into four types, as shown in Table 2, according to Lai et al. and Nie et al. [29,30], and their volume ratios are shown in Table 3. All the pore volume ratios in core #Y1 were slightly larger than those in core #Y2, except for micropores. This reflects the relationship between permeability and pore size to a certain degree, such that the higher the proportion of pores with a larger radius, the greater the permeability.
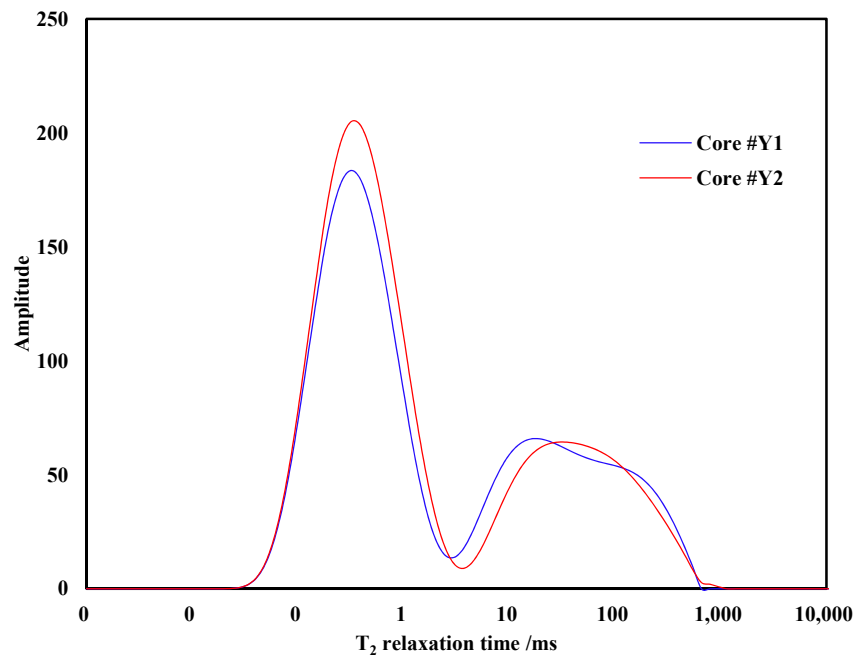
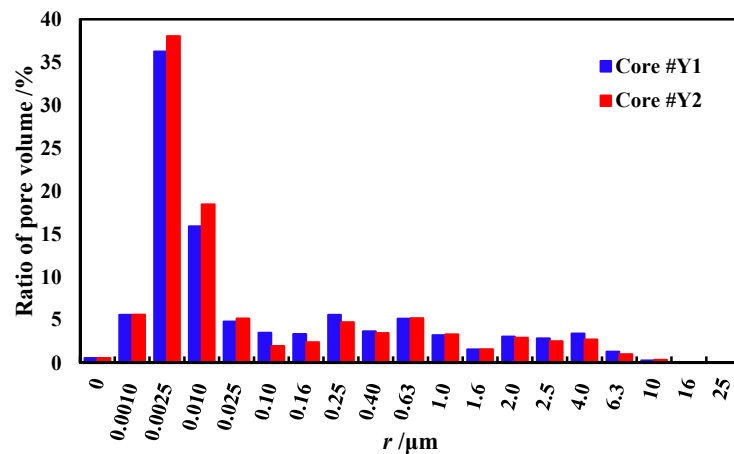**Figure 6.** $T_2$ spectrum curves of initial saturated oil in cores.



**Figure 7.** The histogram of pore radius distribution.

**Table 2.** Relationship between $T_2$, pore radius, and pore type.

| $T_2$ Relaxation Time, ms | Pore Radius, µm | Pore Type |
|:---:|:---:|:---:|
| $T_2 < 1$ | $r < 0.020$ | micropore |
| $1 \leq T_2 < 10$ | $0.020 \leq r < 0.25$ | smallpore |
| $10 \leq T_2 < 100$ | $0.25 \leq r < 2.0$ | mesopore |
| $T_2 \geq 100$ | $r \geq 2.0$ | macropore |

**Table 3.** Pores' volume ratio of different scales (%).

| Core No. | Micropore $<r_1$ | Smallpore $r_1 \leq r < r_2$ | Mesopore $r_2 \leq r < r_3$ | Macropore $\geq r_3$ |
|:---:|:---:|:---:|:---:|:---:|
| Core #Y1 | 56.38 | 13.57 | 19.19 | 10.85 |
| Core #Y2 | 60.26 | 11.93 | 18.29 | 9.53 |

### 4.2. Recovery Factor of CO₂ Huff-n-Puff Process

4.2.1. Effect of Cycle Number

Figure 8 depicts the measured cumulative oil recovery factor (ORF) versus cycle numbers at a pressure of 15 MPa. The results showed that the effect was positive for continental shale oil produced by $CO_2$ huff-n-puff. After five cycles, the cumulative ORFs of cores #Y1 and #Y2 reached 40.34% and 37.66%, respectively. In the first three cycles, the cumulative ORFs significantly increased, and the oil production accounted for 89.80% and 89.53%, respectively, but slowly increased in the succeeding two cycles. Additionally, the cumulative ORFs gradually increased in the natural logarithmic form with cycle number. Correspondingly, as shown in Figure 9, the single cycle ORFs rapidly decreased in the exponential form with cycle number, and the recoveries were only 1.37% and 1.29% for cores #Y1 and #Y2, respectively, at the last cycle. This indicates that the interaction between $CO_2$ and shale oil gradually reduced until it was ineffective for EOR. Thus, based on the analysis of the experimental results, efficient production required about three-to-five cycles of $CO_2$ huff-n-puff for shale oil reservoirs, which was consistent with the research of W. Pu and B. Wei [31].
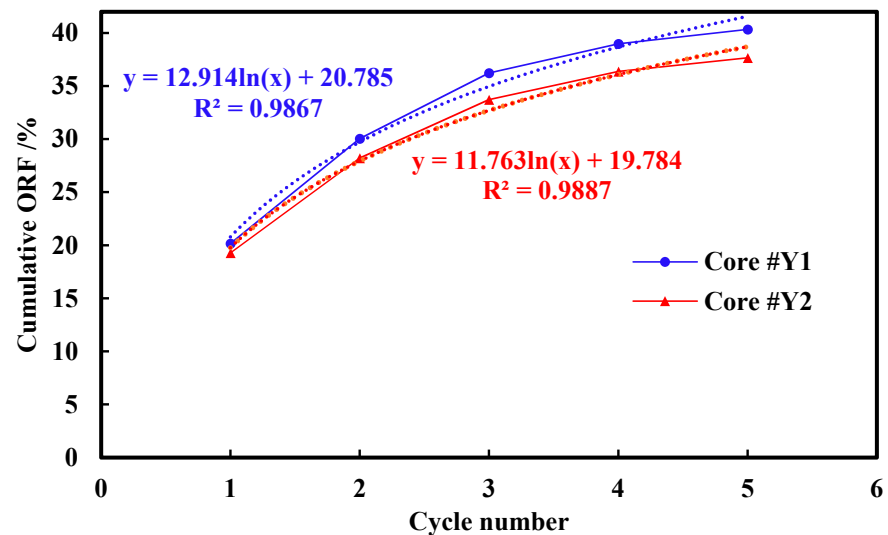


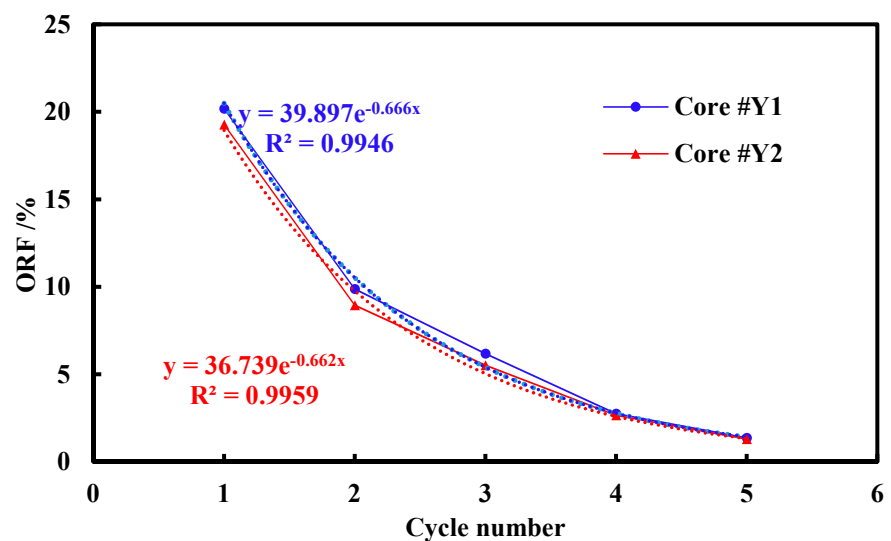**Figure 8.** Cumulative ORF versus cycle numbers.



**Figure 9.** ORF of different $CO_2$ injection cycles.

### 4.2.2. Effect of Permeability

The permeabilities of experimental cores Y1 and Y2 were $0.2911 \times 10^{-3}$ $\mu m^2$ and $0.0169 \times 10^{-3}$ $\mu m^2$, respectively, as seen in Table 1. A series of experiments were carried out to investigate the effect of permeability on the oil recovery factor during the $CO_2$ huff-n-puff process under 15 MPa of pressure, as shown in Figures 8 and 9. The single cycle and cumulative ORF of core #Y1 was larger than those of core #Y2. However, as shown in Figure 10, the differences of single cycle ORFs sharply decreased between the specimens with different permeabilities after two cycles, and it was only 0.07% in the fifth cycle. That was because the permeability was proportional to the pore radius of the reservoir. Under the same external conditions, the larger the permeability and the corresponding average pore radius, the smaller capillary force and seepage resistance; then, the saturation of the movable fluid increased in the pore and the recovery factor of $CO_2$ huff-n-puff was higher. The remaining oil decreased with the permeability increases. Generally, fracturing and acidizing could enlarge the sizes of pores, fractures, and permeability for shale oil reservoirs, thus creating a foundation to improve the recovery by $CO_2$ huff-n-puff.
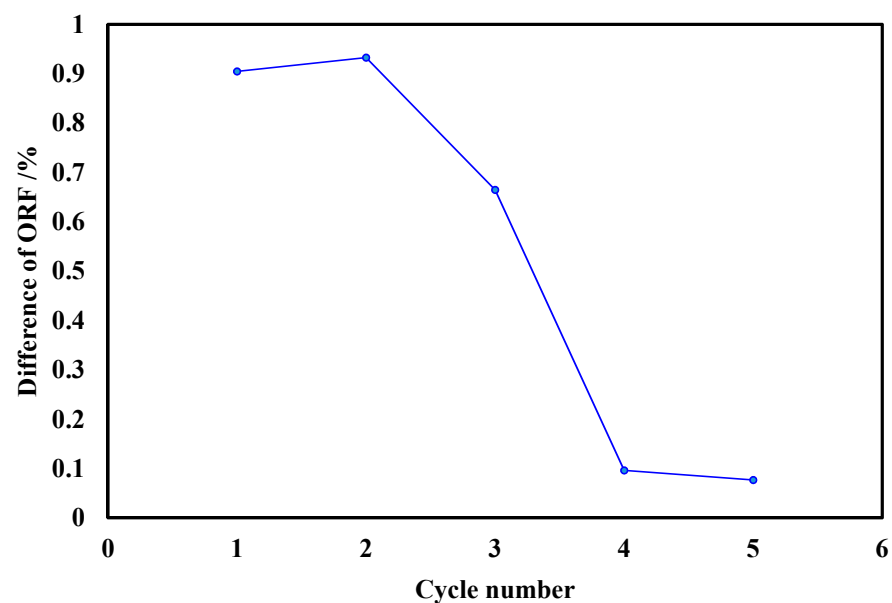


**Figure 10.** Difference of ORF versus different $CO_2$ injection cycles.

### 4.3. Microscopic Process with NMR Tests

Though the recovery factors can be calculated from the experimental data of different $CO_2$ huff-n-puff cycles, it is difficult to quantitatively determine the oil production and remaining oil in different scale pores in a core. However, to investigate the NMR $T_2$ spectrum curves shown in Figure 11, we obtained the characteristics of ORF, the remaining oil distribution in different-scale pores, and the pores' contributions to EOR.

#### 4.3.1. Characteristics of Shale Oil Mobilization

As shown in Figure 11a,b, compared with the initial saturated oil, there are three obvious wave crests in the NMR $T_2$ spectrum curve at the end of each $CO_2$ injection cycle. This confirms that the target reservoir had a strong heterogeneity and once again mainly consisted of four scales of pores. The distribution curves of the $T_2$ spectrum obtained from the $CO_2$ huff-n-puff experiment gradually shift downward to the left with the cycle numbers. The curve with the $T_2$ larger than 10 ms more significantly shifts, indicating that the crude oil flowed out first in the mesopores and macropores, which was consistent with a study of Ma et al. [32].

In the first cycle, the oil production was greatest in the macropores. The percentages of the recovery factor were 36.95% and 39.75% for experimental samples. Following

was mesopores, accounting for 33.53% and 31.85%, and then 24.11% and 16.21% in the smallpores. Finally, the percentages were at the minimum in the micropores, accounting for only 7.10% and 10.51%. However, with the increase of the injection cycles, the oil production proportion of the macropores continuously decreased and more sharply reduced after the third cycle. Additionally, the oil recovery factors of mesopores also obviously decreased after the third cycle but were generally stable in the smallpores. The percentage gradually increased in the micropores, especially more obviously after the third cycle. After five cycles, the average cumulative ORFs of different pores in the two samples were 97.26%, 70.94%, 64.71%, and 13.89%. The oil production percentages in different pores are shown in Table 4. Therefore, with the increase of the cycle numbers, most oil in macropores and mesopores had flowed out, and the oil in smallpores and micropores became the main oil-producing area after approximately three-to-five cycles of $CO_2$ huff-n-puff.

**Table 4.** Percentage of oil production in different pore scales (%).

| Cycle Number | Core #Y1 | | | | Core #Y2 | | | |
|---|---|---|---|---|---|---|---|---|
| | Micro | Small | Meso | Macro | Micro | Small | Meso | Macro |
| | $<r_1$ | $r_1 < r < r_2$ | $r_2 < r < r_3$ | $>r_3$ | $<r_1$ | $r_1 < r < r_2$ | $r_2 < r < r_3$ | $>r_3$ |
| 1 | 7.10 | 24.11 | 31.85 | 36.95 | 10.51 | 16.21 | 33.53 | 39.75 |
| 2 | 18.65 | 20.03 | 35.19 | 26.13 | 27.88 | 18.16 | 43.76 | 10.20 |
| 3 | 24.85 | 13.54 | 53.87 | 7.74 | 38.96 | 19.19 | 29.48 | 12.38 |
| 4 | 50.96 | 24.91 | 23.06 | 1.07 | 64.57 | 19.34 | 15.89 | 0.21 |
| 5 | 55.94 | 28.71 | 14.07 | 1.27 | 70.51 | 18.72 | 10.36 | 0.42 |

### 4.3.2. Characteristics of Remaining Oil Distribution

After quantitatively calculating the NMR $T_2$ spectrum curves shown in Figure 11, we were able to obtain the relationship between the remaining oil in different pore sizes and $CO_2$ huff-n-puff cycle numbers, as shown in Figures 12 and 13. The remaining oil saturation was the highest, and the producing degree was the lowest at end of each gas injection cycle in the micropores. The remaining oil saturation was still as high as 87.63% and 84.59% after the entire experiment in the two cores. The remaining oil saturation values of the medium and smallpores were between those of the micropore and macropore, and they obviously dropped in the first three cycles before basically stabilizing at 26.77~45.03%. The remaining oil saturation was only 2.74%, and the producing degree was very high in the macropores. Additionally, the total remaining oil saturation continuously dropped with the cycle numbers, and the average percentages of the remaining oil saturation in the small, medium, and large pores were 8.35%, 8.90%, and 0.46%, respectively, but the percentage in the micropores gradually increased to 82.29%. This means that, after the $CO_2$ huff-n-puff experiment for continental shale oil, the remaining oil was mainly in the micropores, a little was in the medium and smallpores, and an even smaller amount was in the macropores. This showed that there were great differences in the characteristics of mobilization and remaining oil micro-distribution among different sizes of pores. Consequently, the critical problem of EOR for Chang 7 continental shale oil is how to efficiently develop and reduce the remaining oil in the micropores.
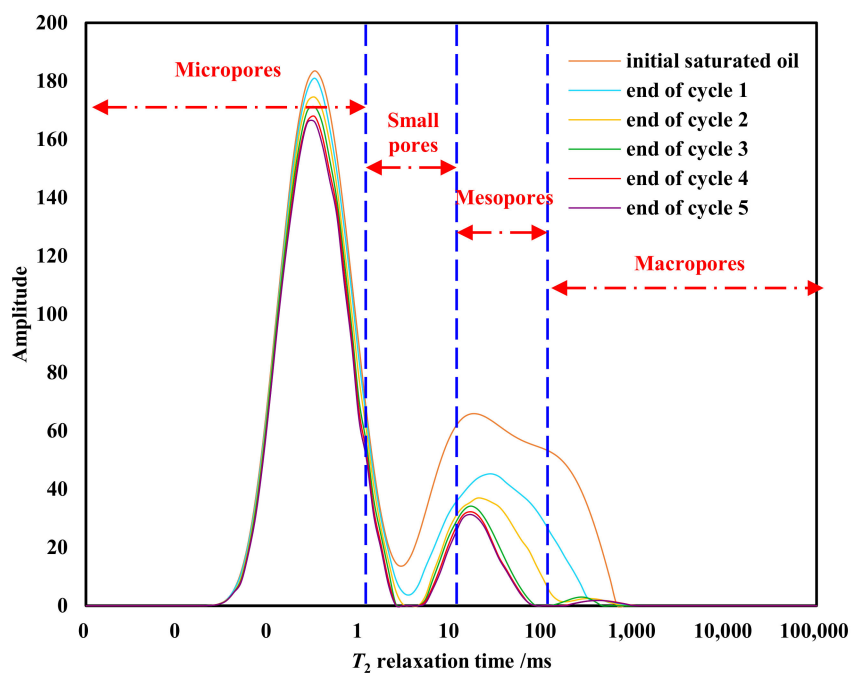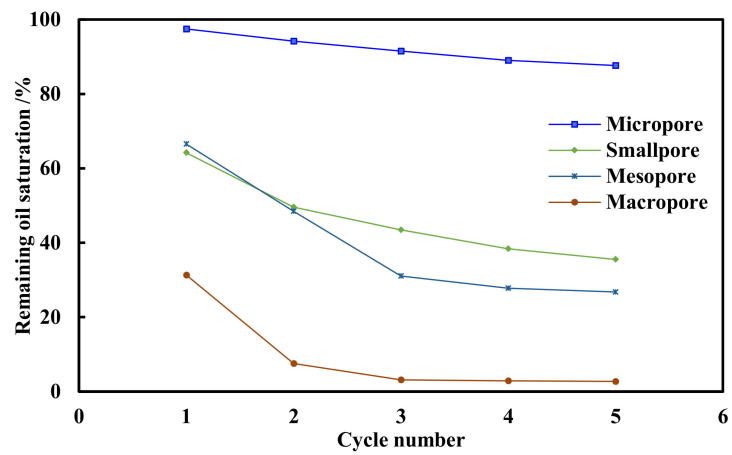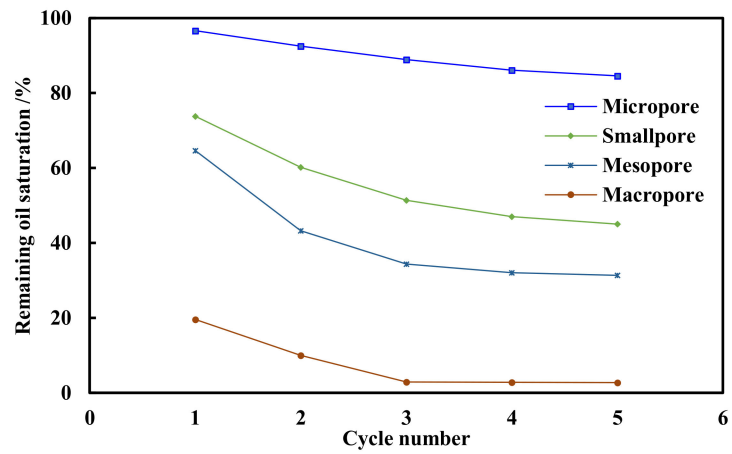
(**a**) Core #Y1
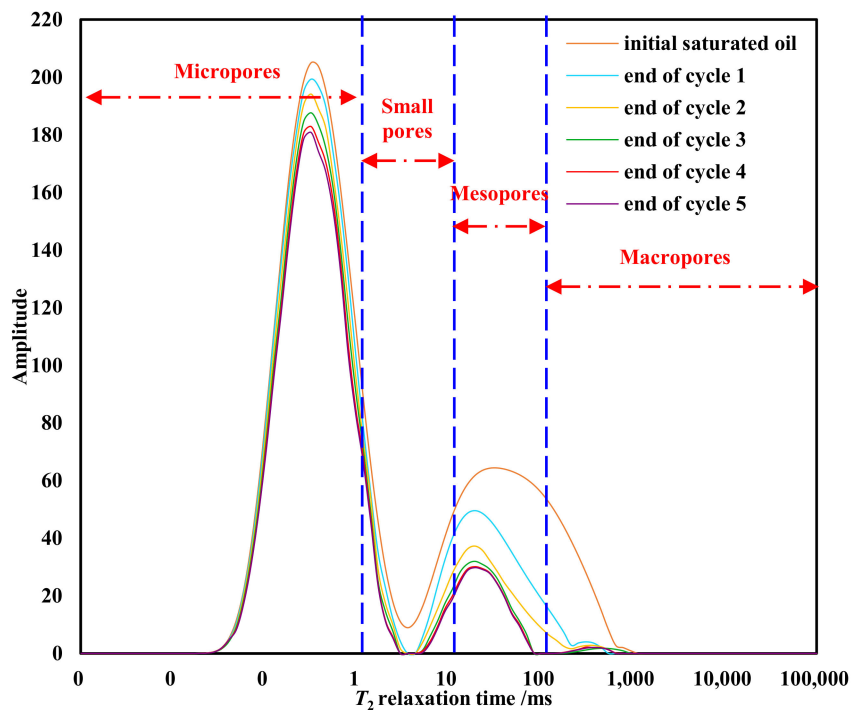


(**b**) Core #Y2

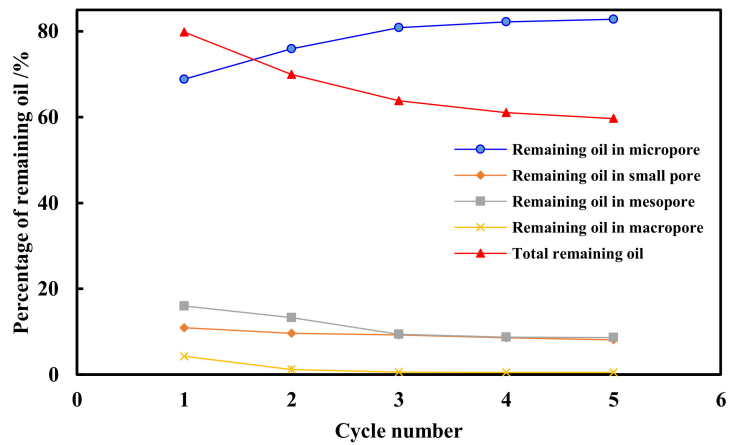**Figure 11.** NMR $T_2$ spectrum curve after different cycles under 15 Mpa.

(**a**) Core #Y1



(**b**) Core #Y2

**Figure 12.** Remaining oil saturation in different pore scales.



(**a**) Core #Y1

**Figure 13.** *Cont.*
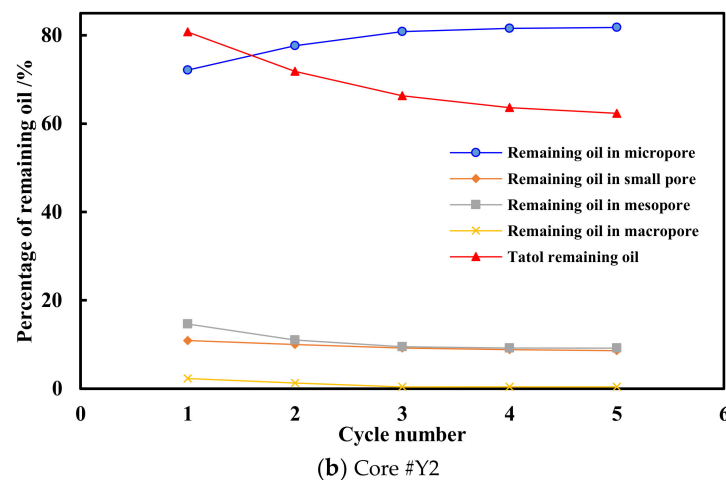
(**b**) Core #Y2

**Figure 13.** Percentage of remaining oil in different pore scales.

## 5. Process and Mechanism Analysis of $CO_2$ Huff-n-Puff

Alfarge et al. [33,34] summarized several mechanisms for injecting $CO_2$ to improve oil recovery in unconventional reservoirs through laboratory experiments and numerical simulations, as shown in Table 5. For one $CO_2$ huff-n-puff cycle, there are three stages: huff, soak, and puff. During huff, $CO_2$ flows into the reservoir and passes through the fractures, and the rock matrix is encompassed by $CO_2$. Then, the $CO_2$ permeates into the rock by differential pressure and concentration. Some oil is carried into the matrix pores by the flow of $CO_2$, but the oil also swells and some is simultaneously extruded out of the pores. During the soaking period, oil further swells and viscosity is further reduced, and the oil migrates toward the fractures. During puff, the bulk fluid (miscible or immiscible oil and $CO_2$) in the matrix flow towards the fracture, and the oil moves from the pores into the fracture via $CO_2$ diffusion caused by the differential pressure and concentration of the gradually reducing $CO_2$.

**Table 5.** The mechanism of $CO_2$-EOR in unconventional reservoirs (Modified on the basis of Alfarge et al. [34] and Lang D. et al. [35]).

| $CO_2$ Mechanism | Approach Tool |
| --- | --- |
| 1: $CO_2$ diffusion and molecular diffusion | Lab and simulation |
| 2: Reduction in Capillary forces | Lab and simulation |
| 3: Dissolution | Lab |
| 4: Replacement | Lab |
| 5: Miscible | Simulation |
| 6: Repressurization | Lab |
| 7: Extraction | Lab |
| 8: Oil swelling and pressure maintenance | Lab and simulation |
| 9: Oil Viscosity reduction | Lab and simulation |
| 10: Combination of more than one mechanism from above | – |

However, we analyzed the results of multiple-cycle $CO_2$ huff-n-puff experiments for the Chang 7 continental shale oil reservoir with an ultra-low matrix permeability and a complex pore structure in this study. Then, the processes and mechanisms could be indicated as follows.

(1)   In the first huff-n-puff cycle, $CO_2$ was preferentially injected into the macropores with smaller capillary resistance under the pressure differential effect. Additionally, $CO_2$ was dissolved in the crude oil to generate oil swelling, pressurization, and viscosity reduction. Then, the oil was rapidly produced. Secondly, a small amount of $CO_2$ entered the mesopores and smallpores to produce a little oil. Finally, a tiny amount of oil was obtained by $CO_2$ with diffusion in micropores.

(2)  With the cycle numbers increased, most of the crude oil in the macropores drained, and then the flow resistance and $CO_2$ consumption in the macropores reduced. Therefore, the concentration of the $CO_2$ that contacted and reacted with the remaining oil in the mesopores and smallpores was relatively higher, and the crude oil could be further extracted. However, as shown in Figure 14 and Table 4, the ORF and the percentage of oil production in meso and smallpores both sharply reduced after three injection cycles in this experiment. Analyses have shown that the proportion of adsorbed oil in such pores is higher than that in macropores [36,37], and after several cycles of $CO_2$ huff-n-puff, the free oil basically discharged but the adsorbed oil was hard to extract.

(3)  For the micropores that accounted for more than half of the total pore volume, the shale oil recovery factor was generally at a low level. As shown in Figure 14, though the ORF was found to be the highest in the second cycle, it was also only 3.27% and 4.14% in the first and second cycles, respectively. An analysis showed that the capillary resistance was very large due to the tiny pore size of the micropores. Then, the $CO_2$ mainly entered into the micropores through diffusion to interact with shale oil. Thus, the total amount and rate of $CO_2$ entering the micropores were both lower. Meanwhile, with the production of shale oil in other pores, more $CO_2$ flowed towards the micropores, and the amount of $CO_2$ diffused into the micropores increased, leading to the free oil with a low proportion to quickly discharge. However, the adsorption effect of micropores was stronger, and the remaining adsorbed oil was more difficult to extract. This resulted in the shale oil recovery factor significantly reducing after two cycles of $CO_2$ huff-n-puff.
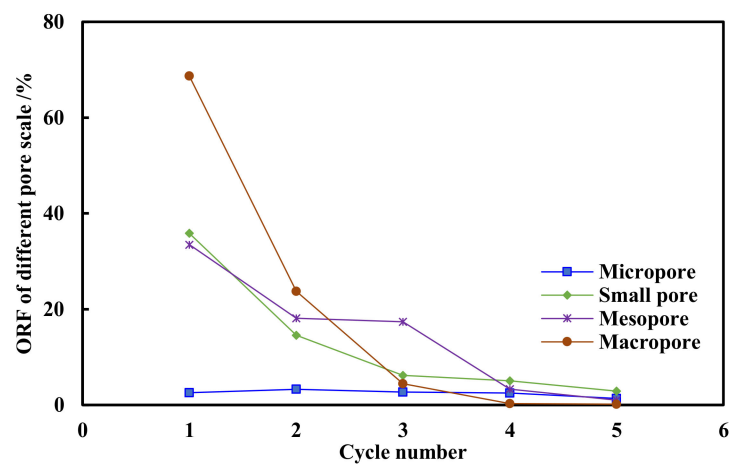


(**a**) Core #Y1
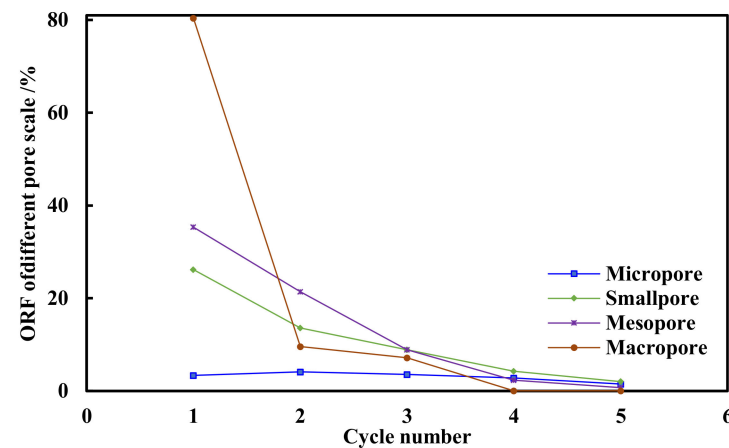


(**b**) Core #Y2

**Figure 14.** ORF of different pore scales versus cycle number.

## 6. Conclusions

In this paper, the Chang 7 continental shale pore characteristics and radius distribution were analyzed by SEM and NMR $T_2$ spectrum curves, and a series of $CO_2$ huff-n-puff experiments and NMR tests were carried out to investigate the shale oil recovery factor with different cycles, characteristics of production, and amounts of remaining oil distribution in different size pores. The main conclusions based on the above experimental results are as follows.

(1)  In order to study the pore structure of Chang 7 continental shale, a series of SEM and NMR tests were conducted. The SEM images showed that there were massive micro-smallpores and fractures, as well as a few large-scale pores. These results qualitatively characterized the complexity of the pore structure. Furthermore, the $T_2$ spectrum curves of saturated oil and remaining oil had two and three wave crests, respectively. We could quantitatively classify the pores into four types, namely micropore, smallpore, mesopore, and macropore. The proportions of the different pore volumes were 56.38% and 60.26%, 13.57% and 11.93%, 19.19% and 18.29%, 10.85%, and 9.53%, respectively, in the two samples. The above results indicated a strong heterogeneity of the Chang 7 continental shale.

(2)  With the huff-n-puff cycle number, the cumulative ORF gradually increased in the natural logarithmic form, and the single-cycle ORF rapidly decreased in the exponential form. Additionally, the fifth cycle was only 1.37% and 1.29%, respectively, for the aforementioned forms. This shows that an economic production comprises about three-to-five cycles for the shale oil reservoir. Additionally, the higher the permeability was, the higher the ORF was found to be. However, each pore was mainly composed of micropores, and the total capillary force and oil flow resistance were higher, resulting in a difference of ORF that was far less than that of permeability between the two experimental samples.

(3)  A battery of NMR $T_2$ spectrum curves of the $CO_2$ huff-n-puff reflected the recovery factors and remaining oil content of different pores. After five cycles, for the experimental samples, the average cumulative ORF of macropores was greater than 97%, and the mesopores, smallpores, and micropores had average cumulative ORFs of 70.94%, 64.71%, and 13.89%, respectively. Meanwhile, the final remaining oil of micropores accounted for 82.29% of the total amount, and the smallpores, mesopores, and large pores accounted for 8.35%, 8.90%, and less than 0.5%, respectively. These results suggest that the remaining oil was mainly in micropores and rarely in macropores. This reflects that there were great differences in the characteristics of mobilization and the remaining oil micro-distribution among different sizes of pores.

(4)  The shale oil was usually stored freely and adsorbed in the pores. However, the proportion of adsorbed oil in the micropores was higher than that in macropores, and the adsorbed oil was hard to extract. Additionally, the $CO_2$ could more easily flow into macropores, mesopores, and smallpores under the pressure differential effect. However, only small amount of $CO_2$ could slowly diffuse into the micropores, resulting the differences of oil production and remaining oil micro-distribution.

(5)  For the Chang 7 continental shale, large-scale fracturing and acidizing may comprise foundation to promote a better contact and reaction between $CO_2$ and shale oil in micropores. Then, one could effectively develop shale oil, reduce remaining oil, and enhance shale oil recovery.

**Conflicts of Interest:** The authors declare no conflict of interest.

## References

1.  Solarin, S.A.; Gil Alana Luis, A.; Lafuente, C. An investigation of long range reliance on shale oil and shale gas production in the U.S. market. *Energy* **2019**, *195*, 116933. [CrossRef]
2.  Energy Information Administration. U.S. Energy Facts—Energy Explained. 2019. Available online: https://www.eia.gov/energyexplained/?page=us_energy_home (accessed on 17 May 2019).
3.  Zhao, W.Z.; Hu, S.Y.; Hou, L.H. Connotation and strategic role of in-situ conversion processing of shale oil underground in the onshore China. *Pet. Explor. Dev.* **2018**, *45*, 537–545. [CrossRef]
4.  Hu, S.; Zhao, W.; Hou, L.; Yang, Z.; Zhu, R.; Wu, S.; Bai, B.; Jin, X. Development potential and technical strategy of continental shale oil in China. *Pet. Explor. Dev.* **2020**, *47*, 819–828. [CrossRef]
5.  Zhao, W.; Hu, S.; Hou, L.; Yang, T.; Li, X.; Guo, B.; Yang, Z. Types and resource potential of continental shale oil in China and its boundary with tight oil. *Pet. Explor. Dev.* **2020**, *47*, 1–11. [CrossRef]
6.  Gamadi, T.D.; Sheng, J.J.; Soliman, M.Y. An experimental study of cyclic gas Injection to Improve shale oil recovery. In Proceedings of the SPE Annual Technical Conference and Exhibition, New Orleans, LA, USA, 30 September–2 October 2013. [CrossRef]
7.  Sun, R.; Yu, W.; Xu, F.; Pu, H.; Miao, J. Compositional simulation of $CO_2$ Huff-n-Puff process in Middle Bakken tight oil reservoirs with hydraulic fractures. *Fuel* **2019**, *236*, 1446–1457. [CrossRef]
8.  Sheng, J.J. Enhanced oil recovery in shale reservoirs by gas injection. *J. Nat. Gas Sci. Eng.* **2015**, *22*, 252–259. [CrossRef]
9.  Sheng, J.J.; Chen, K. Evaluation of the EOR potential of gas and water injection in shale oil reservoirs. *J. Unconv. Oil Gas Resour.* **2014**, *5*, 1–9. [CrossRef]
10. Elwegaa, K.; Emadi, H.; Soliman, M.; Gamadi, T.; Elsharafi, M. Improving oil recovery from shale oil reservoirs using cyclic cold carbon dioxide injection-An experimental study. *Fuel* **2019**, *254*, 115586. [CrossRef]
11. Sheng, J.J.; Mody, F.; Griffith, P.J.; Barnes, W.N. Potential to increase condensate oil production by huff-n-puff gas injection in a shale condensate reservoir. *Nat. Gas Sci. Eng.* **2013**, *28*, 46–51. [CrossRef]
12. Jia, B.; Tsau, J.; Barati, R. A review of the current progress of $CO_2$ injection EOR and carbon storage in shale oil reservoirs. *Fuel* **2019**, *236*, 404–427. [CrossRef]
13. Li, L.; Su, Y.; Hao, Y.; Zhan, S.; Lv, Y.; Zhao, Q.; Wang, H. A comparative study of $CO_2$ and $N_2$ huff-n-puff EOR performance in shale oil production. *J. Pet. Sci. Eng.* **2019**, *181*, 106174. [CrossRef]
14. Li, L.; Sheng, J.J.; Watson, M.; Mody, F. Experimental and Numerical Upscale Study of Cyclic Methane Injection to Enhance Shale Oil Recovery. In Proceedings of the AIChE Annual Conference, Salt Lake City, UT, USA, 8–13 November 2015.
15. Weijermars, R.; Nandlal, K.; Khanal, A.; Tugan, M.F. Comparison of pressure front with tracer front advance and principal flow regimes in hydraulically fractured wells in unconventional reservoirs. *J. Pet. Sci. Eng.* **2019**. [CrossRef]
16. Ho Tuan, A.; Wang, Y. Enhancement of oil flow in shale nanopores by manipulating friction and viscosity. *Phys. Chem. Chem. Phys. PCCP* **2019**, *21*, 1–10.
17. Yu, H.; Qi, S.; Chen, Z.; Cheng, S.; Xie, Q.; Qu, X. Simulation Study of Allied In-Situ Injection and Production for Enhancing Shale Oil Recovery and $CO_2$ Emission Control. *Energies* **2019**, *12*, 3961. [CrossRef]
18. Gamadi Talal, D.; Elldakli, F. Compositional Simulation Evaluation of EOR Potential in Shale Oil Reservoirs by Cyclic Natural Gas Injection. In Proceedings of the SPE/AAPG/SEG Unconventional Resources Technology Conference, Denver, CO, USA, 25–27 August 2014.
19. Li, L.; Sheng James, J. Gas Selection for Huff-n-Puff FOR in Shale Oil Reservoirs Based upon Experimental and Numerical Study. In Proceedings of the SPE Unconventional Resources Conference, Society of Petroleum Engineers, Calgary, AB, Canada, 15–16 February 2017.
20. Tao, W. Evaluate EOR Potential in Fractured Shale Oil Reservoirs by Cyclic Gas Injection. In Proceedings of the Unconventional Resources Technology Conference, Denver, CO, USA, 12–14 August 2013.
21. Wan, T.; Sheng, J. Compositional Modelling of the Diffusion Effect on EOR Process in Fractured Shale-Oil Reservoirs by Gas flooding. *J. Can. Pet. Technol.* **2015**, *54*, 2248–2264. [CrossRef]
22. Gamadi, T.D.; Sheng, J.J.; Soliman, M.Y.; Menouar, H.; Watson, M.C.; Emadibaladehi, H. An experimental study of cyclic $CO_2$ Injection to Improve shale oil recovery. In Proceedings of the SPE Improved Oil Recovery Symposium, Tulsa, OK, USA, 12–16 April 2014. [CrossRef]
23. Zhang, Y.; Yu, W.; Li, Z.; Sepehrnoori, K. Simulation study of factors affecting $CO_2$ huff-n-puff process in tight oil reservoirs. *J. Pet. Sci. Eng.* **2018**, *163*, 264–269. [CrossRef]
24. Wei, B.; Zhong, M.; Gao, K.; Li, X.; Zhang, X.; Cao, J.; Lu, J. Oil recovery and compositional change of $CO_2$ huff-n-puff and continuous injection modes in a variety of dual-permeability tight matrix-fracture model. *Fuel* **2020**, *276*, 117939. [CrossRef]
25. Wang, X.; Xiao, P.; Yang, Z.; Liu, X.-W.; Xia, Z.-Z.; Wang, L.-Q. Laboratory and field-scale parameter optimization of $CO_2$ huff-n-puff with the staged-fracturing horizontal well in tight oil reservoir. *J. Pet. Sci. Eng.* **2019**, *186*, 106703. [CrossRef]
26. Li, J.; Jin, W.; Wang, L.; Wu, Q.; Lu, J.; Hao, S. Quantitative evaluation of organic and inorganic pore size distribution by NMR: A case from the Silurian Longmaxi Formation gas shale in Fuling area, Sichuan Basin. *Oil Gas Geol.* **2016**, *37*, 129–134. [CrossRef]

27. Liu, J.; Sheng, J.J. Experimental investigation of surfactant enhanced spontaneous imbibition in Chinese shale oil reservoirs using NMR tests. *J. Ind. Eng. Chem.* **2018**, *72*, 414–422. [CrossRef]

28. Gu, X.; Pu, C.; Huang, H.; Huang, F.; Li, Y.; Liu, Y.; Liu, H. Micro-influencing mechanism of permeability on spontaneous imbibition recovery for tight sandstone reservoirs. *Pet. Explor. Dev.* **2017**, *44*, 948–954. [CrossRef]

29. Lai, F.; Li, Z.; Wei, Q.; Zhang, T.; Zhao, Q. Experimental investigation of spontaneous imbibition in tight reservoir with nuclear magnetic resonance testing. *Energy Fuels* **2016**, *30*, 8932–8940. [CrossRef]

30. Nie, X.; Chen, J. Nuclear Magnetic Resonance Measurement of Oil and Water Distributions in Spontaneous Imbibition Process in Tight Oil Reservoirs. *Energies* **2018**, *11*, 3114. [CrossRef]

31. Pu, W.; Wei, B.; Jin, F.; Li, Y.; Jia, H.; Liu, P.; Tang, Z. Experimental investigation of $CO_2$ huff-n-puff process for enhancing oil recovery in tight reservoirs. *Chem. Eng. Res. Des.* **2016**, *111*, 13256–13271. [CrossRef]

32. Ma, Q.; Yang, S.; Lv, D.; Wang, M.; Chen, J.; Kou, G.; Yang, L. Experimental investigation on the influence factors and oil production distribution in different pore sizes during $CO_2$ huff-n-puff in an ultra-high-pressure tight oil reservoir. *J. Pet. Sci. Eng.* **2019**, *178*, 1155–1163. [CrossRef]

33. Alfarge, D.; Wei, M.; Bai, B. $CO_2$-EOR mechanisms in huff-n-puff operations in shale oil reservoirs based on history matching results. *Fuel* **2018**, *226*, 112–120. [CrossRef]

34. Alfarge, D.; Wei, M.; Bai, B. Factors affecting $CO_2$-EOR in shale-oil reservoirs: Numerical simulation study and pilot tests. *Energy Fuel* **2017**. [CrossRef]

35. Lang, D.; Lun, Z.; Lyu, C.; Wang, H.; Zhao, Q.; Sheng, H. Nuclear magnetic resonance experimental study of $CO_2$ injection to enhance shale oil recovery. *Pet. Explor. Dev.* **2021**, *48*, 1–10.

36. Zhang, S.; Li, , Y.; Pu, H. Studies of the storage and transport of water and oil in organic-rich shale using vacuum imbibition method. *Fuel* **2020**, *266*, 117096. [CrossRef]

37. Cui, J.; Cheng, L. A theoretical study of the occurrence state of shale oil based on the pore sizes of mixed Gaussian distribution. *Fuel* **2017**, *206*, 564–571. [CrossRef]